

DYNAMIC ANALYSES AND FLIGHT TESTING FOR THE DESIGN OF FLOATING CANARD AIRCRAFT

Naoto Morita[1], Naomi Okubo[2], Takumi Ogawa[2] & Yuto Sasaki[1]

[1]Velocity Aeroworks Inc.
[2]The University of Tokyo

Abstract

This paper investigates the dynamic characteristics and control-system design of a floating canard aircraft, in which the canard surface is freely rotatable in pitch and does not contribute to the static longitudinal stability of the aircraft. A linearized longitudinal dynamic model that explicitly includes the coupling between aircraft pitch motion and canard rotational dynamics is derived, and the aerodynamic derivatives used for control design are estimated from aerodynamic analyses based on an unstructured low-order panel method. An augmented model including actuator lag is then used to construct a model-reference LQI controller and a state observer. Numerical simulations compare the pitch-command responses with and without the observer and under different flight speeds. Flight-test data are also used to evaluate the onboard observer states and to discuss the trim-compensation behavior caused by a difference in the actual canard moment arm. The results show that control-system design for floating canard aircraft must explicitly account for unmeasured internal-state estimation and the speed-dependent variation of dynamic coupling.

Keywords: Floating canard, Aircraft control, Model-reference control

1. Introduction

Conventional canard aircraft are generally constrained by the lift sharing required to ensure the static margin of the complete aircraft. In such configurations, the canard tends to require a higher lift coefficient than the main wing, and the stall margin of the canard can limit the lift coefficient achievable by the main wing.

From the viewpoint of aerodynamic efficiency, it is desirable to operate the main wing at a relatively high lift coefficient in order to use the airfoil performance effectively and reduce the total drag of the aircraft. Therefore, to extend the operating range of the main-wing lift coefficient while retaining the advantages of a canard configuration, the contribution of the canard to the static longitudinal stability must be reconsidered.

Velocity Aeroworks Inc. aims to develop High-Altitude Pseudo-Satellites (HAPS) capable of continuous day-and-night operation, and is conducting research and development on technologies for controlling highly flexible main wings using multiple canard surfaces [1, 2]. In this study, an all-moving canard that is aerodynamically self-balanced is considered as a means of achieving both gust alleviation and reduction of total aircraft drag. Such a canard, which is free to rotate about its hinge axis, is referred to in this paper as a floating canard.

In a floating canard configuration, if dynamic effects are neglected, the pitching moment generated by the canard does not depend on the aircraft angle of attack. Consequently, the canard does not contribute to the static longitudinal stability of the aircraft, and the main-wing lift coefficient may be increased without reducing the overall static margin.

However, introducing a floating canard adds the canard relative angle and relative angular velocity to the longitudinal state variables. Depending on the design parameters, dynamic coupling can occur

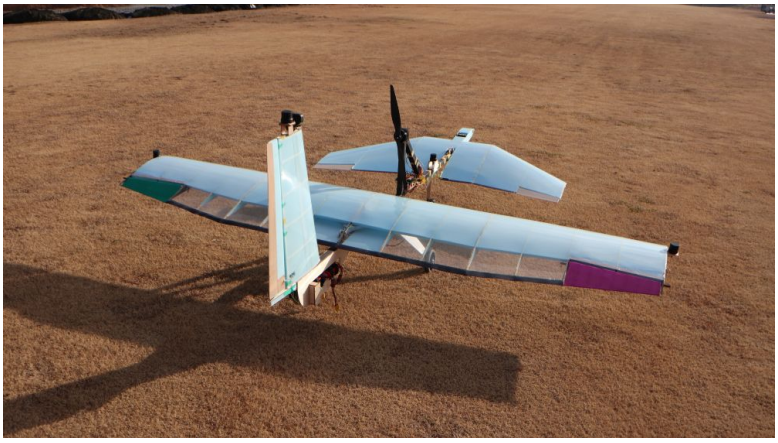


Figure 1 – Experimental aircraft equipped with an all-moving floating canard.

between the aircraft short-period longitudinal mode and the canard rotational mode, potentially reducing pitch damping or causing instability. Therefore, the usefulness of a floating canard configuration cannot be assessed only from static longitudinal stability; the aircraft and canard must be analyzed as a coupled dynamic system.

This paper formulates the longitudinal motion of a floating canard aircraft and derives a linearized state-space representation suitable for analysis and control design. Aerodynamic derivatives are then estimated using an unstructured low-order panel method, and a model-reference LQI controller is constructed using an augmented model that includes actuator lag. Time-response analyses with and without the observer and at different flight speeds, together with flight-test evaluation of the estimated states, are used to clarify control-design issues specific to floating canard aircraft.

2. Formulation of Floating Canard Aircraft Dynamics

The experimental aircraft considered in this study is shown in Fig. 1. The canard is supported by bearings about its hinge axis and is free to rotate in pitch relative to the aircraft body. The aerodynamic moment about the hinge axis depends on the canard angle of attack and the canard pitch rate, as in a conventional aerodynamic control surface.

The canard angle of attack depends not only on the aircraft angle of attack and the canard relative angle, but also on the aircraft pitch rate. When the aircraft has a nose-up pitch rate, an upward velocity component is induced at the canard location, changing the local angle of attack of the canard. This effect excites the canard rotational motion and changes the pitch damping of the longitudinal dynamics.

This section organizes this geometric relation into nonlinear equations of motion and then linearizes the equations about a trimmed flight condition. In particular, the relationship with the aircraft pitch acceleration that appears when the canard relative angle is used as a state variable is made explicit, and the state-space model used for subsequent control design is derived.

The translational and rotational components of the aircraft dynamics are described in the same manner as those of a conventional aircraft, and the relative rotational motion of the canard is added. As a result, the linearized longitudinal dynamics of the floating canard aircraft explicitly include the coupling between aircraft pitch motion and canard rotational motion.

2.1 Physical Model and Coordinate Definition

Figure 2 illustrates the longitudinal model of the floating canard aircraft considered in this study. The aircraft motion is described in the longitudinal plane using the body-axis velocity components u and w, pitch rate q, and pitch attitude angle θ. The aircraft angle of attack is defined as

$$\alpha = \tan^{-1}\left(\frac{w}{u}\right). \tag{1}$$

The floating canard is mounted ahead of the aircraft center of gravity and is free to rotate about its hinge axis. The distance from the aircraft center of gravity to the canard aerodynamic center is

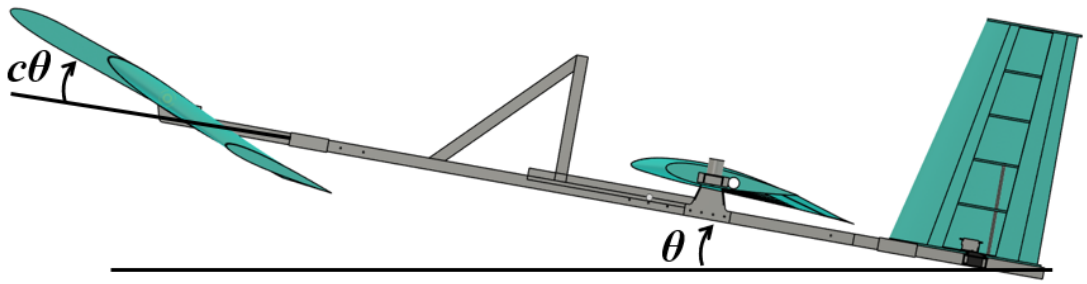


Figure 2 – Definition of the longitudinal model of the floating canard aircraft. The positive direction of the canard angle $c\theta$ is defined as nose-up rotation of the canard.

denoted by L_c. The canard pitch angle relative to the aircraft body is denoted by $c\theta$, and the positive direction of $c\theta$ is defined as nose-up rotation of the canard. The canard angular velocity is denoted by $cq = c\dot{\theta}$.

Due to aircraft rotational motion, the local flow velocity observed by the canard differs from that at the aircraft center of gravity. In particular, the pitch rate q induces an additional vertical velocity component at the canard location. Therefore, the effective angle of attack of the canard is expressed as

$$\alpha_c = \alpha + c\theta - \tan^{-1}\left(\frac{L_c q}{U}\right), \tag{2}$$

where $U = \sqrt{u^2 + w^2}$ is the flight speed. For small perturbations about a trimmed flight condition, this relation can be approximated as

$$\alpha_c \simeq \alpha + c\theta - \frac{L_c}{U_0} q. \tag{3}$$

Equation (3) is a key relation in the present formulation. It shows that the canard angle of attack depends not only on the aircraft angle of attack and the canard pitch angle, but also on the aircraft pitch rate. This pitch-rate-dependent term generates dynamic coupling between the aircraft short-period motion and the canard rotational motion.

2.2 Nonlinear Equations of Motion

The longitudinal motion of the aircraft is formulated using nonlinear equations of motion. In the body-fixed coordinate system, the translational and rotational equations are written as

$$\dot{u} = \frac{X}{m} - qw - g\sin\theta, \tag{4}$$

$$\dot{w} = \frac{Z}{m} + qu + g\cos\theta, \tag{5}$$

$$\dot{q} = \frac{M}{I_y}, \tag{6}$$

$$\dot{\theta} = q, \tag{7}$$

where m is the aircraft mass, I_y is the moment of inertia about the pitch axis, g is the gravitational acceleration, and X, Z, and M are the aerodynamic force components and pitching moment acting on the aircraft.

The rotational motion of the canard is modeled as a single-degree-of-freedom motion about the canard hinge axis. Because $c\theta$ is the relative angle with respect to the aircraft body, the absolute pitch angle of the canard can be written as

$$\eta_c = \theta + c\theta. \tag{8}$$

Then, $\dot{\eta}_c = q + cq$. Considering the relation between the absolute angular acceleration and the relative angular acceleration of the canard gives

$$\dot{c\theta} = cq, \tag{9}$$

$$\dot{cq} = \frac{M_c}{I_c} - \dot{q}, \tag{10}$$

where I_c is the moment of inertia of the canard about the hinge axis and M_c is the aerodynamic hinge moment acting on the floating canard. The term $-\dot{q}$ in Eq. (10) appears because the relative angle $c\theta$ is used as a state variable.
The aerodynamic forces and moments are functions of the aircraft states, control inputs, and canard motion. In particular, the canard hinge moment is modeled as

$$M_c = M_c\left(\alpha_c, cq, \delta_e\right), \tag{11}$$

where δ_e denotes the elevator or servo input applied to the canard. Similarly, the aircraft pitching moment is expressed as

$$M = M\left(u, \alpha, q, c\theta, cq, \delta_T\right), \tag{12}$$

where δ_T denotes the throttle input.
These nonlinear equations describe the physical origin of the dynamic coupling. A perturbation in the aircraft pitch rate changes the local angle of attack of the canard through Eq. (2). The resulting hinge moment changes the canard pitch angle, and the changed canard angle further modifies the pitching moment acting on the aircraft. Therefore, even when the floating canard does not contribute to static longitudinal stability, it can strongly affect dynamic stability.

2.3 Linearization about a Trimmed Flight Condition

The nonlinear equations are linearized about a steady trimmed flight condition. The trim condition is defined as

$$u = U_0, \quad \alpha = \alpha_0, \quad q = 0, \quad \theta = \theta_0, \quad cq = 0, \quad c\theta = c\theta_0. \tag{13}$$

Small perturbations from the trim condition are introduced as

$$u = U_0 + \Delta u, \quad \alpha = \alpha_0 + \Delta\alpha, \quad q = \Delta q, \quad \theta = \theta_0 + \Delta\theta, \quad cq = \Delta cq, \quad c\theta = c\theta_0 + \Delta c\theta. \tag{14}$$

Neglecting higher-order perturbation terms, the perturbation in the canard angle of attack becomes

$$\Delta\alpha_c = \Delta\alpha + \Delta c\theta - \frac{L_c}{U_0}\Delta q. \tag{15}$$

Using the relative angular acceleration, the linearized canard rotational equation is written as

$$\Delta\dot{cq} = H_\alpha \Delta\alpha_c + H_{cq}\Delta cq + H_{\delta_e}\Delta\delta_e - \Delta\dot{q}. \tag{16}$$

The last term in Eq. (16) originates from the fact that $c\theta$ is the angle relative to the aircraft body.
The aircraft pitching moment is also linearized about the trim condition as

$$\Delta\dot{q} = M_u\Delta u + M_\alpha\Delta\alpha + M_q\Delta q + M_{c\theta}\Delta\alpha_c - Arm_{\mathrm{T}}X_{dT}\frac{m}{I_y}\Delta\delta_T. \tag{17}$$

Substituting Eq. (15) into Eq. (17) gives

$$\Delta\dot{q} = M_u\Delta u + \left(M_\alpha + M_{c\theta}\right)\Delta\alpha + \left(M_q - \frac{L_c}{U_0}M_{c\theta}\right)\Delta q + M_{c\theta}\Delta c\theta - Arm_{\mathrm{T}}X_{dT}\frac{m}{I_y}\Delta\delta_T. \tag{18}$$

This equation shows that the floating canard modifies not only the apparent pitch stiffness but also the pitch damping term. Therefore, the dynamic behavior of the aircraft cannot be evaluated from static longitudinal stability alone, and the aircraft and canard must be analyzed as a higher-order coupled dynamic system.

Substituting Eqs. (15) and (18) into Eq. (16), the linearized equation for the relative canard angular velocity becomes

$$\Delta \dot{cq} = -M_u \Delta u + (H_\alpha - M_\alpha - M_{c\theta})\Delta\alpha + \left(-\frac{L_c}{U_0}H_\alpha - M_q + \frac{L_c}{U_0}M_{c\theta}\right)\Delta q + H_{cq}\Delta cq + (H_\alpha - M_{c\theta})\Delta c\theta + H_{\delta_e}\Delta\delta_e \tag{19}$$

Equation (19) corresponds directly to the fifth row of the state matrix introduced in the next subsection. In particular, the coupling from the aircraft pitch rate to the relative canard angular acceleration includes not only the term $-L_c H_\alpha \Delta q/U_0$ originating from the local canard angle of attack, but also the terms $-M_q\Delta q + L_c M_{c\theta}\Delta q/U_0$ that arise from subtracting the aircraft pitch acceleration.

2.4 Matrix Representation of the State Equation

The linearized state-space model used in this study is

$$\dot{x} = Ax + Bu. \tag{20}$$

The state and input vectors are defined as

$$x = \begin{bmatrix} u & \alpha & q & \theta & cq & c\theta \end{bmatrix}^\mathsf{T}, \qquad u = \begin{bmatrix} \delta_e & \delta_T \end{bmatrix}^\mathsf{T}. \tag{21}$$

The system matrix A and input matrix B are given by

$$A = \begin{bmatrix} X_u & X_\alpha & X_q & -g & 0 & 0 \\ \dfrac{Z_u}{U_0} & \dfrac{Z_\alpha}{U_0} & \dfrac{Z_q}{U_0}+1 & 0 & 0 & 0 \\ M_u & M_\alpha + M_{c\theta} & M_q - \dfrac{L_c}{U_0}M_{c\theta} & 0 & 0 & M_{c\theta} \\ 0 & 0 & 1 & 0 & 0 & 0 \\ -M_u & H_\alpha - M_\alpha - M_{c\theta} & -\dfrac{L_c}{U_0}H_\alpha - M_q + \dfrac{L_c}{U_0}M_{c\theta} & 0 & H_{cq} & H_\alpha - M_{c\theta} \\ 0 & 0 & 0 & 0 & 1 & 0 \end{bmatrix}, \tag{22}$$

$$B = \begin{bmatrix} 0 & X_{dT} \\ 0 & 0 \\ 0 & -Arm_\mathrm{T} X_{dT}\dfrac{m}{I_y} \\ 0 & 0 \\ H_{\delta_e} & 0 \\ 0 & 0 \end{bmatrix}.$$

Equations (20)–(22) explicitly represent the coupling between the relative rotational dynamics of the floating canard and the longitudinal motion of the aircraft. Based on this model, the aerodynamic estimation of the linearized coefficients is discussed in the next section.

3. Aerodynamic Derivative Estimation

The aerodynamic derivatives included in Eq. (22) are estimated using aerodynamic analyses and small-perturbation analyses with UNLSI. UNLSI is an in-house unstructured low-order panel-method solver used in this study [3]. In this solver, the aircraft surface is represented by an unstructured surface mesh, and low-order singularity distributions are placed on each panel to satisfy the non-penetration boundary condition on the aircraft surface. The pressure coefficient is obtained from the resulting surface velocity distribution and integrated over the aircraft surface to evaluate the aerodynamic force and moment coefficients about the body axes.

In the representative full-aircraft analysis, the reference area, reference span, reference chord, and moment reference point were set to $S_\mathrm{ref} = 1.5\,\mathrm{m}^2$, $b_\mathrm{ref} = 2.8\,\mathrm{m}$, $c_\mathrm{ref} = 0.54\,\mathrm{m}$, and $x_\mathrm{ref} = [-0.02, 0, 0]\,\mathrm{m}$, respectively. Propeller-induced velocity was not considered, the laminar ratio was set to 0.4, and the representative velocity was set to $10\,\mathrm{m/s}$. In the static analyses with varying angle of attack, the geometric rotation of the canard surface was applied in the direction opposite to the aircraft angle of

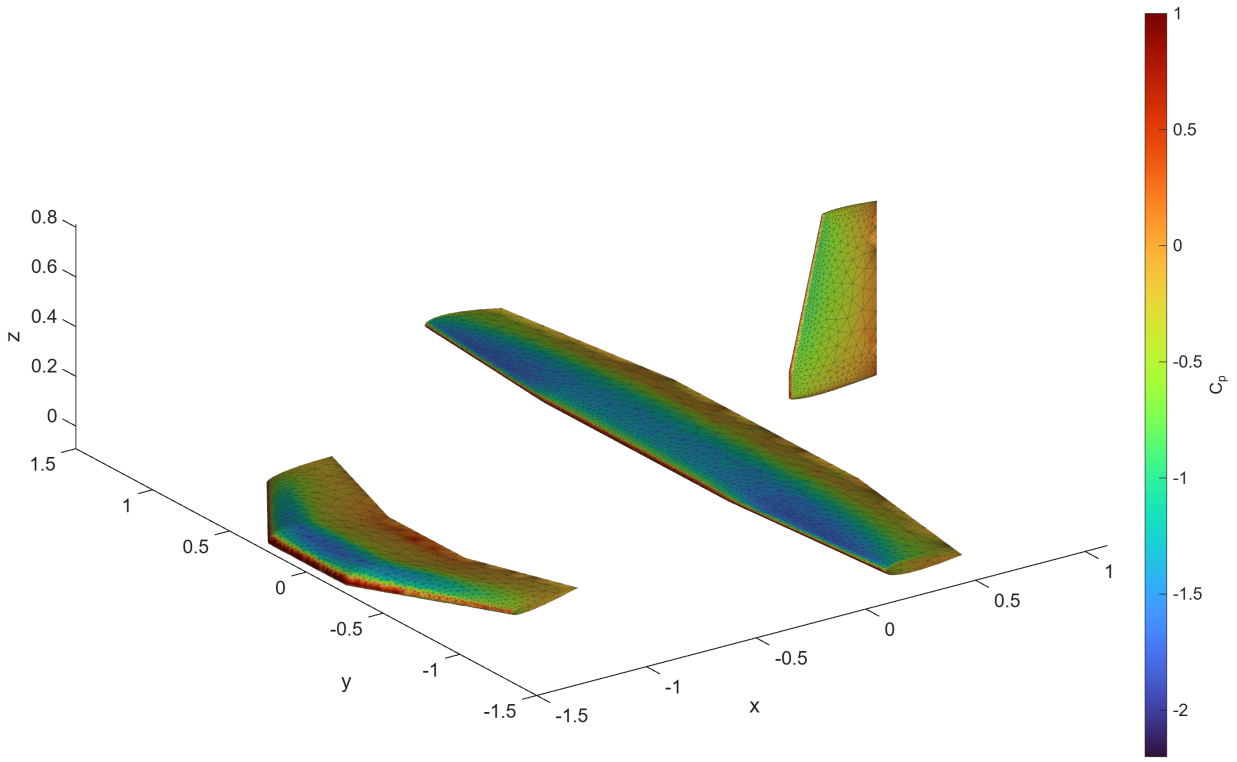


Figure 3 – Full-aircraft C_p distribution obtained using UNLSI. The analysis condition is $\alpha = 0\,\mathrm{deg}$, $\beta = 0\,\mathrm{deg}$, $M = 0.001$, and $Re = 3.0 \times 10^5$.

attack so that the treatment of the canard relative angle was consistent with the formulation in the previous section.

Figure 3 shows a representative full-aircraft C_p distribution at $\alpha = 0\,\mathrm{deg}$. The displayed range of pressure coefficient is $[-2.2, 1]$, and the pressure distribution is evaluated for the complete aircraft geometry including the main wing, floating canard, and vertical tail.

The dynamic stability derivatives are evaluated using central differences with small perturbations in angle of attack, sideslip angle, and angular rates about the reference flow condition. Let the aerodynamic coefficient vector be

$$C = \begin{bmatrix} C_X & C_Y & C_Z & C_l & C_m & C_n \end{bmatrix}^{\mathsf{T}}. \tag{23}$$

The derivative with respect to a generalized variable ξ is evaluated as

$$\frac{\partial C}{\partial \xi} \simeq \frac{C(\xi + \Delta\xi) - C(\xi - \Delta\xi)}{2\Delta\xi}. \tag{24}$$

Here, ξ represents β, α, $\hat{p}$, $\hat{q}$, or $\hat{r}$. As in conventional aircraft derivative definitions, the angular rates are nondimensionalized as

$$\hat{p} = \frac{p b_{\mathrm{ref}}}{2U_0}, \qquad \hat{q} = \frac{q c_{\mathrm{ref}}}{2U_0}, \qquad \hat{r} = \frac{r b_{\mathrm{ref}}}{2U_0}. \tag{25}$$

In the present calculation, the perturbation step was set to $\Delta\xi = \varepsilon^{1/3}$ considering the balance between machine round-off error and finite-difference truncation error. Aerodynamic analyses were conducted for each perturbation condition, and the resulting differences in aerodynamic coefficients were substituted into Eq. (24) to evaluate derivatives with respect to β, α, p, q, r, and control-surface deflections.

The coefficient database used for the linear model was constructed from multiple analysis points with varying angle of attack, sideslip angle, and control-surface deflections. At each point, both static aerodynamic coefficients and dynamic stability derivatives were evaluated, and the resulting discrete data were arranged in a form that can be continuously evaluated by multidimensional interpolation. For the control analyses, derivatives such as $C_{X\alpha}$, $C_{Z\alpha}$, $C_{m\alpha}$, C_{Xq}, C_{Zq}, and C_{mq} were extracted from

this interpolation database at the trim point and converted into the linearized coefficients in Eq. (22). Therefore, the aerodynamic derivatives used in the control-response analyses are based on the coefficient database obtained from UNLSI small-perturbation analyses, rather than on empirical assumptions.

4. Aircraft Control System

For the floating canard aircraft, internal states associated with the free rotation of the canard appear in the longitudinal dynamics. Therefore, the control system cannot be adequately represented by a low-order model that treats only the aircraft attitude. In particular, changes in aircraft angle of attack and pitch rate modify the local angle of attack of the canard, resulting in mutual interaction between the canard rotational motion and the aircraft pitching moment.
In this section, the six-state longitudinal model derived in Section 2. is combined with the aerodynamic derivatives estimated in Section 3., and actuator lags of the elevator and throttle are added to construct an augmented model. Based on this augmented model, a model-reference LQI control system that generates the reference response to a pitch-angle command and an observer that estimates unmeasured internal states are designed.

4.1 Overall Control Architecture

The control system used in this study consists of an outer loop and an inner loop. The outer loop generates the pitch-angle command θ_{cmd} from pilot input or guidance commands. In the inner loop, the model-reference LQI controller generates the reference response corresponding to this pitch-angle command and computes the control inputs so that the estimated augmented state follows the reference state.
The longitudinal control inputs are the elevator command δ_e and throttle command δ_T. Since lateral control is not the main subject of this paper, only its outline is described. In the lateral direction, stabilization is performed based on the roll angle and angular rate, and the roll-angle command for turning or path following is generated using the L1 guidance law [4].

4.2 Control Plant Model

The linearized longitudinal model derived in Section 2. is used for controller design. First, the six states of the aircraft and floating canard are defined as

$$x = \begin{bmatrix} \Delta u & \Delta\alpha & \Delta q & \Delta\theta & \Delta cq & \Delta c\theta \end{bmatrix}^T. \tag{26}$$

Here, Δu is the perturbation in forward velocity, $\Delta\alpha$ is the angle-of-attack perturbation, Δq is the pitch-rate perturbation, and $\Delta\theta$ is the pitch-angle perturbation. The variables Δcq and $\Delta c\theta$ represent the perturbations in canard angular velocity and canard angle, respectively.
The control input command is defined as

$$v = \begin{bmatrix} \Delta\delta_{e,\mathrm{cmd}} & \Delta\delta_{T,\mathrm{cmd}} \end{bmatrix}^T, \tag{27}$$

where $\Delta\delta_{e,\mathrm{cmd}}$ and $\Delta\delta_{T,\mathrm{cmd}}$ are the elevator and throttle commands. In the implementation, first-order actuator lags are included as

$$\begin{aligned} \Delta\dot{\delta}_{e,a} &= -\frac{1}{\tau_e}\Delta\delta_{e,a} + \frac{1}{\tau_e}\Delta\delta_{e,\mathrm{cmd}}, \\ \Delta\dot{\delta}_{T,a} &= -\frac{1}{\tau_T}\Delta\delta_{T,a} + \frac{1}{\tau_T}\Delta\delta_{T,\mathrm{cmd}}. \end{aligned} \tag{28}$$

Therefore, the augmented state used for control design is

$$x_m = \begin{bmatrix} x^T & \Delta\delta_{e,a} & \Delta\delta_{T,a} \end{bmatrix}^T, \tag{29}$$

and the augmented linear model is expressed as

$$\dot{x}_m = A_m x_m + B_m v. \tag{30}$$

In the numerical analyses, $\tau_e = 0.05\,\mathrm{s}$ and $\tau_T = 0.01\,\mathrm{s}$ were used.

The directly available measurements in this control system are assumed to be the forward velocity, pitch rate, and pitch angle. Therefore, the measured output is defined as

$$y = \begin{bmatrix} \Delta u & \Delta q & \Delta\theta \end{bmatrix}^T = C_y x_m. \tag{31}$$

The angle of attack, canard angular velocity, canard angle, and actuator states are included in the control model but are not treated as directly measured quantities. These internal states are therefore estimated by the observer described below.
With this structure, the dynamic coupling caused by the free rotation of the canard can be treated as internal states of the control plant model rather than as external disturbances. This is the main difference between the present control system and conventional pitch-attitude stabilization control.

4.3 Model-Reference LQI Control

In this study, model-reference LQI tracking control is used for the longitudinal inner loop. In a conventional state-feedback controller, the control input is applied directly in response to the pitch-angle command. In the present control system, however, a reference model is included inside the controller, and the aircraft response is controlled to follow this reference response.
Let the reference state be x_{ref}. The reference model is given by

$$\dot{x}_{\mathrm{ref}} = A_m x_{\mathrm{ref}} + B_m v_{\mathrm{nom}}. \tag{32}$$

Here, v_{nom} is the nominal input generated from the pitch-angle command and throttle feedforward, and is expressed as

$$v_{\mathrm{nom}} = K_\theta \theta_{\mathrm{cmd}} + u_{\mathrm{ff}} - K_{\mathrm{ref}} x_{\mathrm{ref}}. \tag{33}$$

K_θ is the feedforward gain from the target pitch angle to the elevator and throttle, and u_{ff} is the throttle feedforward term.
The control input applied to the aircraft is computed from the difference between the reference state and the estimated state as

$$v = v_{\mathrm{nom}} - K(\hat{x} - x_{\mathrm{ref}}) - K_i z. \tag{34}$$

Here, $\hat{x}$ is the estimated augmented state from the observer, K is the state-feedback gain obtained from the LQI design, K_i is the integral gain, and z is the integral state of the tracking error.
This control law makes the closed-loop system follow the desired longitudinal response generated by the linearized model, rather than simply tracking the pitch-angle command itself. Because the transient response of the canard angle affects the aircraft pitch response in a floating canard aircraft, introducing a reference model allows the response shape to be prescribed explicitly.

4.4 Integral Compensation

In the actual aircraft, uncertainties exist in the aerodynamic coefficients, center-of-gravity location, canard friction, servo neutral position, and thrust characteristics. Therefore, state feedback based only on the linear model can leave steady-state errors with respect to the target pitch angle or pitch rate. To reduce these steady-state errors, integral compensation is introduced for the tracking errors in pitch rate and pitch angle.
The tracking error is defined as

$$e_x = \hat{x} - x_{\mathrm{ref}}, \tag{35}$$

and the integrated output is defined as

$$C_i e_x = \begin{bmatrix} \Delta q \\ \Delta\theta \end{bmatrix}. \tag{36}$$

The integral state z is updated by

$$\dot{z} = C_i e_x - \lambda_i z, \tag{37}$$

where λ_i is the leakage coefficient of the integrator. The leakage term suppresses excessive accumulation of the integral state during long-duration flight.

The augmented state including the integral state is

$$x_a = \begin{bmatrix} e_x \\ z \end{bmatrix}. \tag{38}$$

The state-feedback gain K and integral gain K_i are obtained simultaneously by solving the LQI problem for this augmented system. This design is based on the framework of linear quadratic optimal control [5]. The cost function is

$$J = \int_0^\infty \left(e_x^T Q e_x + z^T Q_i z + v^T R v \right) dt. \tag{39}$$

Here, Q is the weight on the state deviation, Q_i is the weight on the integral error, and R is the weight on the control input. In the numerical analyses, the state weighting matrix was set to

$$Q = \mathrm{diag}\left(1,\, 10^{-6},\, 1,\, 1,\, 1,\, 1,\, 10^{-5},\, 10^{-5}\right), \tag{40}$$

with $Q_i = 10I$ and $R = \mathrm{diag}(120, 20)$.

4.5 State Observer

In this control system, the canard angle and canard angular velocity are not measured directly. The augmented state is therefore estimated using an observer based on the linearized model [6]. The measurements are the forward velocity, pitch rate, and pitch angle, and the observation equation is given by Eq. (31).

The observer is constructed as

$$\dot{\hat{x}} = A_m \hat{x} + B_m v + L\left(y_o - C_o \hat{x}\right), \tag{41}$$

where L is the observer gain. Weak pseudo-observations are introduced for states that are not directly measured. Specifically, in addition to the directly measured output y, pseudo-observations that weakly pull the unmeasured states toward zero are introduced as

$$y_o = \begin{bmatrix} y \\ 0 \end{bmatrix}, \qquad C_o = \begin{bmatrix} C_y \\ C_p \end{bmatrix}. \tag{42}$$

The standard deviation of the pseudo-observations was set to 0.5, and the standard deviations of the measurement noise in forward velocity, pitch rate, and pitch angle were set to $0.05\,\mathrm{m/s}$, $0.02\,\mathrm{rad/s}$, and $0.02\,\mathrm{rad}$, respectively. The observer gain was designed using the weight $Q_n = 10^{-3}I$ corresponding to the model-noise covariance and the weight R_n corresponding to the measurement-noise covariance.

4.6 Relation to the Onboard State Estimator

In addition to the observer used inside the controller, the actual aircraft implements an onboard state estimator for sensor fusion. This onboard estimator uses sensor information from the IMU, barometric altimeter, pitot tube, GPS or differential GPS, and other sensors to estimate the aircraft attitude, angular rates, position, velocity, and airspeed. For attitude estimation, an error-state Kalman filter formulation based on quaternion kinematics is used [7].

The longitudinal controller receives the forward velocity, pitch rate, and pitch angle obtained from the onboard state estimator. Thus, the onboard state estimator estimates the flight state from actual sensors, while the observer inside the model-reference LQI controller estimates the augmented state including the floating canard and actuators based on those measured quantities.

By separating the state estimator for sensor fusion from the observer based on the control model, the use of actual sensor information and the state estimation required for control design are clearly distinguished.

4.7 Altitude and Lateral Control

During autonomous flight, the pitch-angle command is generated from the altitude error and then input to the model-reference LQI controller. Coupling between altitude control and speed hold in longitudinal autopilot design has been systematized as the Total Energy Control System (TECS), which separates total energy and energy distribution [8]. In the present implementation, this concept is simplified, and the target pitch angle is generated from the altitude error and airspeed error. Let h be the altitude, h_{cmd} the target altitude, V the airspeed, and V_{ref} the reference airspeed. The target pitch angle is then generated as

$$\theta_{\mathrm{cmd}} = K_h \left(h_{\mathrm{cmd}} - h\right) - K_V \left(V_{\mathrm{ref}} - V\right). \tag{43}$$

Here, K_h is the gain for altitude error and K_V is the correction gain for airspeed error. The second term is introduced to suppress excessive nose-up commands during airspeed decrease and to balance altitude control and speed hold.

In the lateral control system, stabilization is performed based on roll angle and roll rate. During turning or path-following flight, the L1 guidance law generates the lateral acceleration command, which is converted into a roll-angle command. Let the lateral acceleration command be a_y. The roll-angle command is then given by

$$\phi_{\mathrm{cmd}} = \tan^{-1}\left(\frac{a_y}{g}\right). \tag{44}$$

Because the main subject of this paper is the stabilization of longitudinal motion including the floating canard, lateral control is treated as an outer loop required to enable autonomous flight.

4.8 Implementation Features

The proposed control system is executed in real time on the onboard computer. Numerical integration is used to update the reference model and observer states, and fourth-order Runge–Kutta integration is used in the implementation to balance numerical accuracy and real-time computation. The control inputs are converted into elevator, throttle, aileron, and rudder commands and then output to the servos and motor.

Saturation is applied to the control inputs considering aircraft and actuator constraints. Immediately after the model-reference control mode is enabled, the reference state and integral state are initialized to suppress transient input growth during mode switching.

With this structure, the control system is designed to compensate for the dynamic coupling in the longitudinal motion including the free rotation of the floating canard, while maintaining a degree of robustness against model errors and sensor noise in the actual aircraft.

5. Analysis Results

This section evaluates the closed-loop response of the model-reference LQI control system constructed in the previous section through numerical simulation. The evaluation focuses on the response difference with and without the state observer and on the sensitivity of the closed-loop response to flight speed. This separates the effects of unmeasured state estimation and speed dependence, both of which are important in the control design of floating canard aircraft.

5.1 Comparison with and without the Observer

First, the effect of the state observer on control performance is evaluated. Both the design speed and plant speed are set to $U_0 = 12\,\mathrm{m/s}$. A model error with a standard deviation of 20% is applied to the aerodynamic derivatives of the plant. White measurement noise with standard deviations of $0.05\,\mathrm{m/s}$, $0.02\,\mathrm{rad/s}$, and $0.02\,\mathrm{rad}$ is also added to the measured forward velocity, pitch rate, and pitch angle, respectively.

Figure 4 shows the response to a pitch-angle command of $0.2\,\mathrm{rad}$. Without the observer, the closed-loop response remains stable, but high-frequency oscillations remain in the pitch rate and canard relative angle because measurement noise enters the feedback directly. With the observer, the effect of measurement noise is reduced by model-based state estimation, and both the initial overshoot and

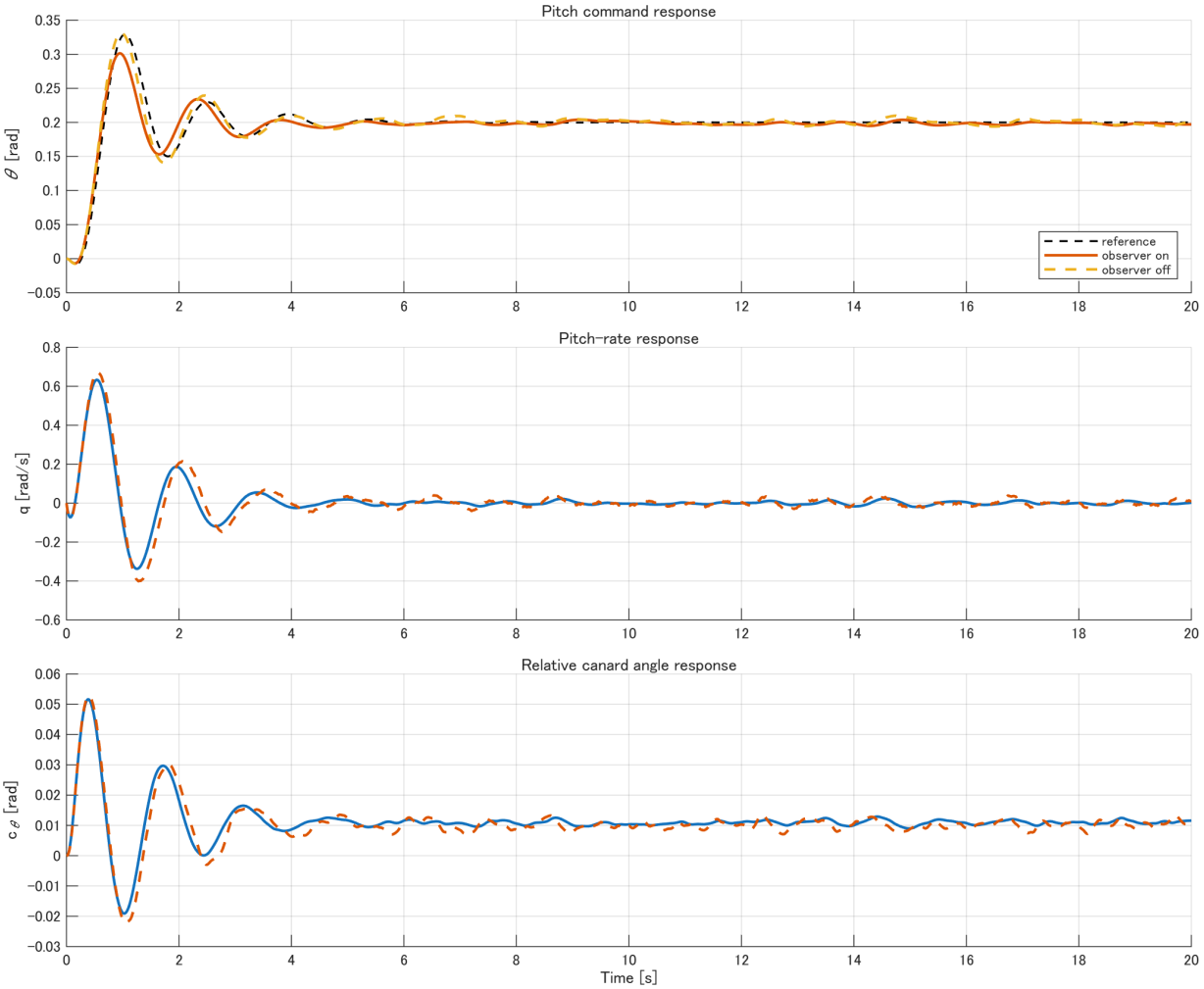


Figure 4 – Comparison of model-reference LQI control with and without the observer. The plant includes 20% aerodynamic-derivative error and measurement noise.

the small-amplitude oscillations after settling are reduced. Therefore, for a control plant that includes unmeasured internal states of the floating canard, observer-based state estimation is effective for shaping the closed-loop response and suppressing noise.

5.2 Effect of Flight Speed

Next, the effect of flight speed on the closed-loop response is evaluated. The controller and reference model are designed at $U_0 = 12\,\mathrm{m/s}$, while only the flight speed of the plant linear model is changed to $U_0 = 10, 12, 14\,\mathrm{m/s}$. To clarify the speed effect, aerodynamic-coefficient errors and measurement noise are not added in this analysis.

Figure 5 shows the response to a pitch-angle command of $0.2\,\mathrm{rad}$. At the design speed of $12\,\mathrm{m/s}$, the response follows the reference model and settles within several seconds. When the flight speed is decreased to $10\,\mathrm{m/s}$, the steady value of the canard relative angle increases and the rise of the pitch-angle response becomes slower. This is because the effective gains of the canard hinge moment and aircraft pitching moment decrease as the dynamic pressure decreases. In contrast, at $14\,\mathrm{m/s}$, the initial response becomes faster, while the overshoot in pitch angle and pitch rate increases.

These results indicate that the closed-loop response of the floating canard aircraft depends strongly on flight speed. Therefore, rather than applying a gain designed at a single speed directly over a wide speed range, robustness evaluation including speed variation or gain scheduling should be considered.

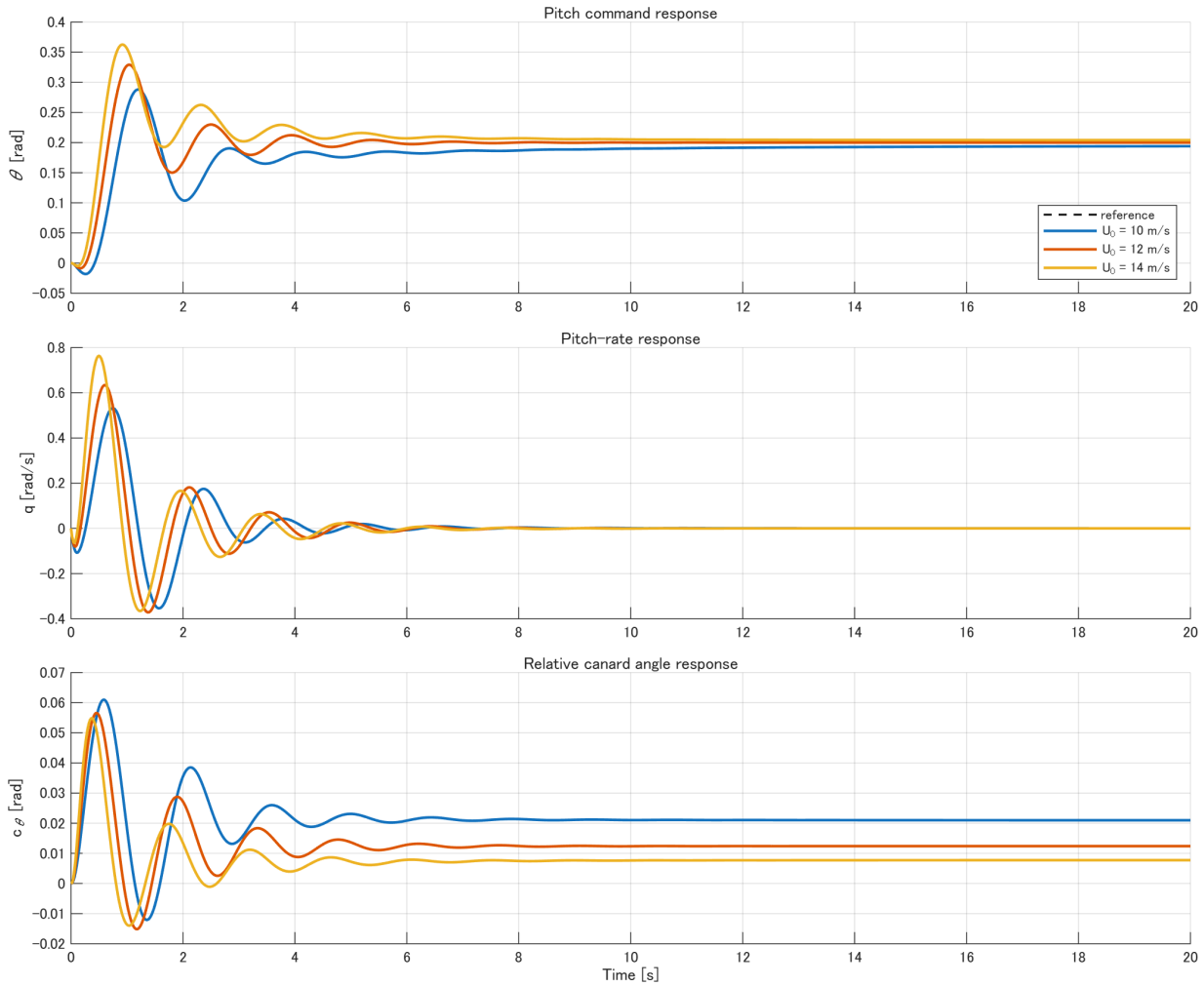


Figure 5 – Pitch-command responses of the model-reference LQI controller at different flight speeds. The controller is designed at $U_0 = 12\,\mathrm{m/s}$, and only the flight speed of the plant model is changed.

6. Flight Test Results

Flight-test data obtained on May 26, 2026 were analyzed to evaluate the actual operation of the proposed control system and observer. The median logging period was approximately $108\,\mathrm{ms}$, indicating that state estimation was executed at a rate sufficient for real-time evaluation during flight. The six recorded estimated states correspond to the states of the linearized longitudinal model defined in Eq. (26). Specifically, the evaluation targets are velocity perturbation, angle-of-attack perturbation, pitch-rate perturbation, pitch-angle perturbation, canard relative angular-velocity perturbation, and canard relative-angle perturbation.

Figure 6 shows the time histories of the observer states with respect to the start time of the log. The measured velocity perturbation was computed as $V_{\mathrm{air}} - U_0$ using the airspeed V_{air} and the design speed $U_0 = 12\,\mathrm{m/s}$. Similar to the measured value obtained from the airspeed, the estimated velocity perturbation Δu transitions from a large negative value near the ground to a small positive value during flight, and then returns to the negative side during the landing or deceleration phase. This trend indicates that the observer captures the main time variation of the speed change. The angle-of-attack perturbation $\Delta\alpha$ transitions from negative to positive during acceleration and fluctuates mostly within approximately 0.05–$0.15\,\mathrm{rad}$ during flight.

The pitch-rate state Δq and pitch-angle state $\Delta\theta$ contain transient variations similar to those in the pitch-rate and pitch-angle measurements derived from the IMU, but do not coincide exactly. This is because the observer states are defined as estimated states about the trim point of the linearized model, rather than as the absolute attitude or raw angular rate themselves. Nevertheless, the estimated values during flight do not diverge and remain bounded until the final phase in which the

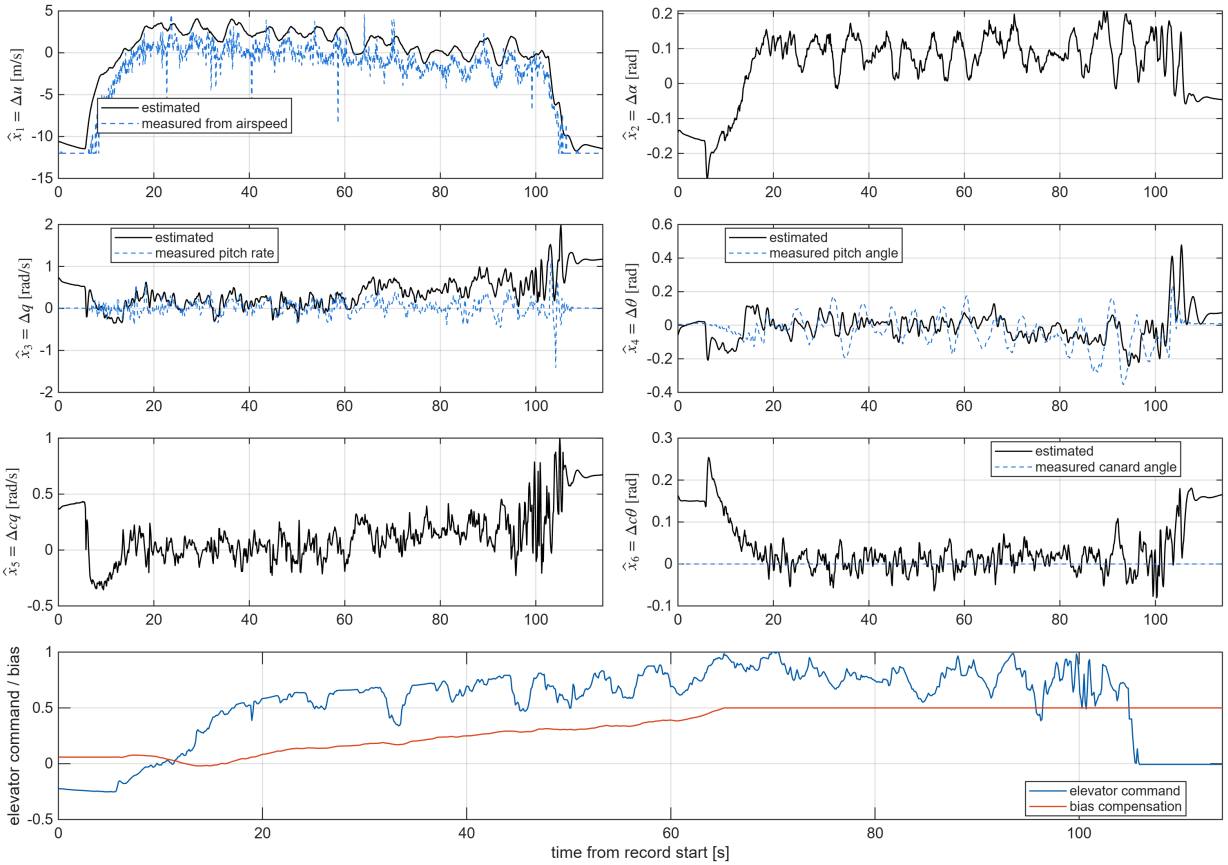


Figure 6 – Observer estimated states based on flight-test data. For the velocity perturbation, the measured value obtained by subtracting the design speed from the airspeed is also shown. The bottom panel shows the elevator command and bias-compensation amount.

airspeed begins to decrease. The canard angular velocity Δcq and canard relative angle $\Delta c\theta$ also remain small during the main flight segment, while larger variations appear in the final low-speed, large-control-deflection segment.

The elevator bias-compensation amount gradually increases during flight and saturates near its upper limit in the latter half of the flight. Post-flight inspection revealed that the actual canard moment arm was approximately $100\,\mathrm{mm}$ shorter than the value used in the design model. This difference is estimated to have reduced the effective gain of the aircraft pitching moment with respect to canard angle or elevator command, requiring additional elevator bias to maintain trim. Therefore, the increase in the bias-compensation amount can be interpreted as the integral compensation absorbing not only uncertainties in servo neutral position and center-of-gravity location, but also the geometric discrepancy in the canard moment arm. The flight-test results show that the onboard observer can continue real-time state estimation, while also indicating that future work should update the model to reflect the actual geometric parameters and retune the trim bias.

7. Conclusion

This study investigated a floating canard configuration as a means of enabling high-lift-coefficient operation of the main wing in a canard aircraft. A linearized model using the canard relative rotation angle as a state variable was derived, and the coupling between aircraft pitch motion and canard rotational motion was incorporated into a state-space representation. Aerodynamic derivatives used in the control-response analyses were estimated using small-perturbation analyses based on an unstructured low-order panel method.

An augmented model including actuator lag was then used to construct a model-reference LQI control system and observer. The comparison with and without the observer showed that, for a plant including unmeasured internal states, model-based state estimation is effective for noise suppression and response shaping. The response analyses with different flight speeds confirmed that the pitch-angle response, pitch-rate response, and canard relative-angle response change when the flight speed deviates from the design speed.

The flight-test data analysis confirmed that the onboard observer can continue real-time state estimation and that, in the actual aircraft, bias compensation absorbed the trim offset caused by the difference in the canard moment arm. These results show that control-system design for floating canard aircraft must explicitly account for unmeasured internal-state estimation and for changes in dynamic pressure and dynamic coupling associated with flight-speed variation.

References

[1] Naoto Morita, Shinichi Nakasuka, Takeshi Tsuchiya, Kazuki Takashima, Yasuyuki Taguchi, Kaito Suzuki, Takashi Koyama, Ren Eto, and Ichiro Baba. Development of multi-canard uav for active aeroelastic control toward pseudo-small satellites. In *Proceedings of the 29th Congress of the International Council of the Aeronautical Sciences (ICAS 2022)*, pages 1–14, ICAS Archive, 2022. ICAS.

[2] C. E. Cesnik, P. J. Senatore, W. Su, E. M. Atkins, and C. M. Shearer. X-hale: A very flexible unmanned aerial vehicle for nonlinear aeroelastic tests. *AIAA Journal*, 50(12):2820–2833, 2017.

[3] UTokyoTsuchiyaLAB. UNLSI: Unstructured low-order source-doublet panel method solver. `https://github.com/UTokyoTsuchiyaLAB/UNLSI`, 2023. Accessed 15 June 2026.

[4] Sanghyuk Park, John Deyst, and Jonathan P. How. A new nonlinear guidance logic for trajectory tracking. In *AIAA Guidance, Navigation, and Control Conference and Exhibit*, Providence, RI, 2004. American Institute of Aeronautics and Astronautics. AIAA Paper 2004-4900, `https://doi.org/10.2514/6.2004-4900`.

[5] R. E. Kalman. Contributions to the theory of optimal control. *Boletin de la Sociedad Matematica Mexicana*, 5(2):102–119, 1960.

[6] D. G. Luenberger. Observing the state of a linear system. *IEEE Transactions on Military Electronics*, 8(2):74–80, 1964. `https://doi.org/10.1109/TME.1964.4323124`.

[7] Joan Sola. Quaternion kinematics for the error-state kalman filter. *arXiv preprint arXiv:1711.02508*, 2017.

[8] A. A. Lambregts. Vertical flight path and speed control autopilot design using total energy principles. In *AIAA Guidance and Control Conference*, Gatlinburg, TN, 1983. American Institute of Aeronautics and Astronautics. AIAA Paper 83-2239, `https://doi.org/10.2514/6.1983-2239`.

Copyright Statement

The authors confirm that they, and/or their company or organization, hold copyright on all of the original material included in this paper. The authors also confirm that they have obtained permission, from the copyright holder of any third party material included in this paper, to publish it as part of their paper. The authors confirm that they give permission, or have obtained permission from the copyright holder of this paper, for the publication and distribution of this paper as part of the ICAS proceedings or as individual off-prints from the proceedings.